

Li-doped Beryllonitrene for Enhanced Carbon Dioxide Capture

Andrew Pu and Xuan Luo

National Graphene Research and Development Center, Springfield, Virginia 22151, USA

(Dated: October 7, 2021)

Abstract

In recent years, the scientific community has given more and more attention to the issue of climate change and global warming, which is largely attributed to the massive quantity of carbon dioxide emissions. Thus, the demand for a carbon dioxide capture material is massive and continuously increasing. In this study, we perform first-principle calculations based on density functional theory to investigate the carbon dioxide capture ability of pristine and doped beryllonitrene. Our results show that carbon dioxide had an adsorption energy of -0.046 eV on pristine beryllonitrene, so it appears that beryllonitrene has extremely weak carbon dioxide adsorption ability. Pristine beryllonitrene could be effectively doped with Lithium atoms, and the resulting Li-doped beryllonitrene had much stronger interactions with carbon dioxide than pristine beryllonitrene. The adsorption energy for carbon dioxide on Li-doped beryllonitrene was -0.408 eV. The adsorption of carbon dioxide on Li-doped beryllonitrene greatly changed the charge density, projected density of states, and band structure of the material, demonstrating that it was strongly adsorbed. This suggests that Li-doping is a viable way to enhance the carbon dioxide capture ability of beryllonitrene and makes it a possible candidate for an effective CO₂ capture material.

I. INTRODUCTION

Climate change has been an important issue facing the world since the 20th century, and research has shown that this is largely a result of the increase in greenhouse gas emissions¹. The majority of these greenhouse gas emissions are from carbon dioxide (CO₂). In 2016, CO₂ accounted for about 81.6% of all manmade greenhouse gas emissions in the US². Global warming caused by the increase in greenhouse gas emissions has caused the arctic ice caps to melt, resulting in higher sea levels³. Rising temperatures also increase the prevalence of droughts and heatwaves, which are both significant threats to the safety of mankind⁴. Thus, the demand for a material to efficiently capture CO₂ from the air has been massive. Currently, there are 3 main methods for CO₂ capture: pre-combustion, post-combustion, and oxyfuel⁵. When applied to the burning of fossil fuels, pre-combustion and oxyfuel CO₂ capture are both performed before CO₂ is actually released into the air, while post-combustion CO₂ capture refers to the process of capturing CO₂ from the resulting gas mixtures. Thus, post-combustion CO₂ capture methods are more applicable to the issue of capturing existing greenhouse gasses from the atmosphere⁶.

Previously, several materials and processes for post-combustion CO₂ capture have been explored. Two of the most promising methods of post combustion CO₂ capture are chemical absorption and adsorption⁷. Amine scrubbing, which is one process used for chemical absorption CO₂ capture, has been practiced since its patent in 1930⁸. However, chemical absorption processes usually require large equipment, large volumes of solvent, high regeneration energy, and toxic byproducts⁹. On the other hand, several adsorbents have been researched for their CO₂ capture ability⁷. Many chemical CO₂ adsorbents have been studied, including several amine-based adsorbents, but their low CO₂ capacity and high cost have reduced their viability⁷. Meanwhile, several different physical adsorbents have also been explored and research, including porous coal, carbonaceous material, zeolite, fullerenes, and MOFs^{7,10}. Many studies have been performed to investigate the possibility of pressure and temperature regulated CO₂ capture using physical adsorbents^{11,12}. However, for all adsorptive CO₂ capture methods, the gaseous feed must be treated, and the gaseous mixture usually has to be cooled and dried¹³. Since the discovery of graphene in 2004, two-dimensional materials have also gathered lots of interest as physical CO₂ adsorbents¹⁴.

Two-dimensional materials have a large surface area, atomic-thin structure, and a large surface-to-volume ratio, making them great potential candidates for CO₂ capture¹⁵. Unfortunately, previous experiments have shown that pristine graphene doesn't demonstrate particularly strong interactions with CO₂¹⁶. This has prompted other researchers to investigate the possibility of two-dimensional materials other than graphene for carbon dioxide capture. Hexagonal boron nitride has a very similar structure to graphene, but it displays greater thermal conductivity, and the nitrogens are believed to be potential active sites for carbon dioxide chemisorption¹⁷. Jiao et al performed density functional theory calculations to investigate this but found that pristine hexagonal boron nitride monolayers were also ineffective for carbon dioxide adsorption. Silicene and germanene were thought to be potential materials because unlike graphene and boron nitride, they have a buckled hexagonal structure, which gives them greater chemical reactivity¹⁸. Both pristine silicene and pristine germanene only demonstrated physisorption with CO₂^{19,20}. Monolayer molybdenum disulfide (MoS₂) was also investigated due to its unique triple layered buckled structure²¹. Like the other two-dimensional materials, pristine MoS₂ also did not display much adsorption ability for CO₂, so it cannot be directly used as an efficient sorbent for CO₂²². Several other two-dimensional materials have been investigated for their CO₂ capture ability, including aluminum nitride²³, zinc oxide²⁴, gallium nitride²⁵, silicon phosphide²⁶, silicon carbide²⁷, graphyne²⁸⁻³⁰, borophene³¹, and several different carbon nitrides³²⁻³⁵. However, most of these 2D materials are unable to strongly chemisorb CO₂ while in their pristine form. On the other hand, other studies have found that dopants and defects were able to greatly increase the adsorption capabilities of many of these 2D materials. Li et al and Chandra et al both found that graphene's CO₂ capture ability was greatly increased after nitrogen doping^{36,37}. Boron nitride was shown to have increased CO₂ adsorption behavior after fluorine doping and boron vacancies^{17,38}. Silicene and Germanene both displayed much greater CO₂ capture ability after Li-functionalization^{18,39}, and MoS₂ monolayers with S vacancies also demonstrated much better adsorption ability²¹. Recently, Bykov et al discovered a new two-dimensional material known as beryllonitrene, which could be a potential CO₂ capture material due to its unusual structure and variety of binding sites⁴⁰.

Beryllonitrene is a monolayer form of BeN₄ that was created by performing high-pressure synthesis followed by decompression on triclinic BeN₄⁴⁰. Not much research has

been conducted regarding its practical applications, including in the field of gas capture and gas sensing. Beryllonitrene is similar to the previously stated two-dimensional materials in that its structure is close to a honeycomb structure, and it has a hexagonal unit cell⁴¹. Each unit cell consists of one beryllium atom and four nitrogen atoms, so the material is mostly composed of nitrogen⁴¹. Like in boron nitride, these nitrogens could act as potential carbon dioxide adsorption sites¹⁷. Beryllonitrene has been shown to be both dynamically and thermodynamically stable⁴⁰. The monolayer exhibits semimetallic behavior⁴¹ and has a large surface area, similar to other two-dimensional materials, making it a good candidate for CO₂ adsorption. Due to the unique properties and lack of research for beryllonitrene, it is important to investigate the potential of beryllonitrene for CO₂ capture.

In this study, we use density functional theory to calculate the adsorption of CO₂ molecules onto the surface of pristine beryllonitrene and Li-doped beryllonitrene in order to determine whether they have the potential to be effectively used as a CO₂ capture device.

II. METHODS

A. Computational Details

First-principle calculations using density functional theory (DFT)^{42,43} as implemented in the ABINIT program⁴⁴⁻⁴⁹ were performed using the generalized gradient approximation (GGA) with the Perdew-Burke-Ernzerhof (PBE) formalism as the exchange-correlation functional⁵⁰. Projector augmented-wave (PAW)^{51,52} pseudopotentials were selected, which were generated by ATOMPAW code⁵³. The electron configurations and radius cutoffs used for generating the PAW pseudopotentials are listed in Table I.

Convergence calculations were performed to determine appropriate converged values for the kinetic energy cutoff, k point mesh, and vacuum. The values were considered converged when the difference in total energy between two data sets was less than 1.0×10^{-4} Ha two times consecutively. During the convergence calculations, the self-consistent field (SCF) total energy calculations were considered complete when the total energy difference was less than 1.0×10^{-10} Ha twice. For the relaxation of the lattice parameters and atomic structure, the Broyden-Fletcher-Goldfarb-Shanno (BFGS) method⁵⁴ was used. During the BFGS relaxation calculations, the SCF iteration was terminated when the total difference in forces

TABLE I: Electron configurations and radial cut offs for all elements used to generate PAW pseudopotentials

Element	Electron Configuration	r_{cut} (bohr)
Beryllium (Be)	1s2 2s2	1.6
Nitrogen (N)	[He] 2s2 2p3	1.2
Aluminum (Al)	[Ne] 3s2 3p1	1.9
Phosphorus (P)	[Ne] 3s2 3p3	1.9
Sulfur (S)	[Ne] 3s2 3p4	1.9

was less than 2.0×10^{-5} Ha/bohr two times consecutively. The BFGS relaxation calculations were considered complete when all of the forces were less than 2.0×10^{-4} Ha/bohr.

B. CO₂ Adsorbed on Pure Beryllonitrene

Convergence calculations were performed on a 1×1 unit cell of beryllonitrene, shown in Figure 1(a), and then converged values were used for relaxation of the atomic structure. Convergence and relaxation calculations were also performed on a single carbon dioxide molecule. Calculations for the adsorption of carbon dioxide on beryllonitrene were performed using a 2×2 supercell of beryllonitrene.

The adsorption energy of CO₂, E_{ads} , on each material was calculated by

$$E_{ads} = E_{ber+CO_2} - E_{ber} - E_{CO_2} \quad (1)$$

where E_{CO_2} , E_{ber} , and E_{ber+CO_2} represent the total energy for isolated carbon dioxide, pristine or doped beryllonitrene, and the carbon dioxide and beryllonitrene complex, respectively.

C. CO₂ Adsorbed on Doped Beryllonitrene

Convergence and relaxation calculations were also performed for 2×2 supercells of doped beryllonitrene. Calculations for the adsorption of carbon dioxide on the doped beryllonitrene were also performed, and the adsorption energy was found using Equation 1.

The defect formation energy, E_{def} , for each doped beryllonitrene monolayer is defined by

$$E_{def} = E_{ber+dop} - E_{ber} - E_{dop} \quad (2)$$

where E_{ber} , E_{dop} , and $E_{ber+dop}$ represent the total energy for pristine beryllonitrene, the interstitial dopant (Li, Ca, or Al) in its crystalline structure, and the doped beryllonitrene, respectively.

D. Electronic Structure

The charge transfer, $\Delta\rho(\tau)$, involved in the adsorption of CO_2 was calculated by

$$\Delta\rho(\tau) = \rho_{ber+CO_2}(\tau) - \rho_{ber}(\tau) - \rho_{CO_2}(\tau) \quad (3)$$

where $\rho_{CO_2}(\tau)$, $\rho_{ber}(\tau)$, and $\rho_{ber+CO_2}(\tau)$ represent the charge density of carbon dioxide, beryllonitrene, and the carbon dioxide and beryllonitrene complex, respectively.

The band structure was calculated for each beryllonitrene monolayer and each complex using Γ , X, M, A, and Y as the high symmetry k points, as shown in Figure 1(b). The tetrahedron method was used to plot the projected density of states (PDOS) for the different monolayers and complexes. The PDOS graphs use the 2s orbital for lithium and beryllium, as well as the 2p orbitals for carbon, nitrogen, and oxygen.

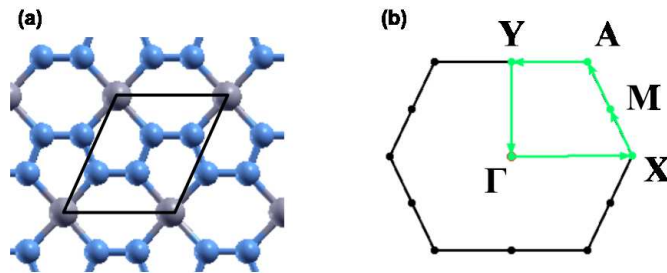


FIG. 1: (a) Atomic structure of pristine beryllonitrene. The black frame indicates a 1×1 cell (b) First Brillouin zone for beryllonitrene with high symmetry points Γ , X, M, A, and Y⁵⁵.

III. RESULTS & DISCUSSION

In this study, we first optimized the structure of beryllonitrene, Li-doped beryllonitrene, and a single carbon dioxide molecule. We then calculated the adsorption energy of carbon dioxide on each of the monolayers. The carbon dioxide was considered chemisorbed when the absolute value of the adsorption energy was greater than the chemisorption threshold of -0.30 eV, which is equivalent to -0.011 Ha^{10,23}.

A. Atomic Structure

The optimized atomic structures for the materials were found using BFGS relaxation calculations, which gives the molecules free range of motion and any bonds formed were chemical bonds⁵⁴.

1. Pristine Beryllonitrene and Carbon Dioxide Structure

TABLE II: Comparison between calculated and previous theoretical values for the lattice parameters (a, b) of beryllonitrene, the bond lengths of the Be-N, N₁-N₂, and N₂-N₂ bond in beryllonitrene, and the C-O bond in carbon dioxide (Atom labels shown in Figure 2)

	a	b	Be-N	N ₁ -N ₂	N ₂ -N ₂	C-O
Calculated (Å)	3.660	4.270	1.747	1.341	1.337	1.172
Theoretical (Å)	3.66 ⁵⁵	4.27 ⁵⁵	1.748 ⁵⁵	1.343 ⁵⁵	1.338 ⁵⁵	1.161 ⁵⁶

Beryllonitrene consists of chains of nitrogen atoms held together by beryllium atoms. The atomic structure is comprised of BeN₄ pentagons and Be₂N₄ hexagons, as shown in Figure 2(a). Table II presents the structural properties of the relaxed beryllonitrene, as well as the bond length of carbon dioxide, and compares them with previous theoretical results. The unit cell of pristine beryllonitrene was optimized and found to have lattice parameters of 3.66 and 4.27 Å. The hexagonal primitive cell has a 64.64° angle between the lattice vectors, which is consistent with previous results⁵⁵. The beryllium-nitrogen bond lengths were found to be approximately 1.75 Å, and the nitrogen-nitrogen bond lengths were all around 1.34 Å,

which is also consistent with previous results⁴¹. The Be-N₁-N₂ bond angle is approximately 131.56°, and the N₁-N₂-N₂ bond angle is approximately 111.49°. A carbon dioxide molecule was also structurally optimized and found to have a linear structure with bond lengths of 1.17 Å, as shown in Figure 2(b).

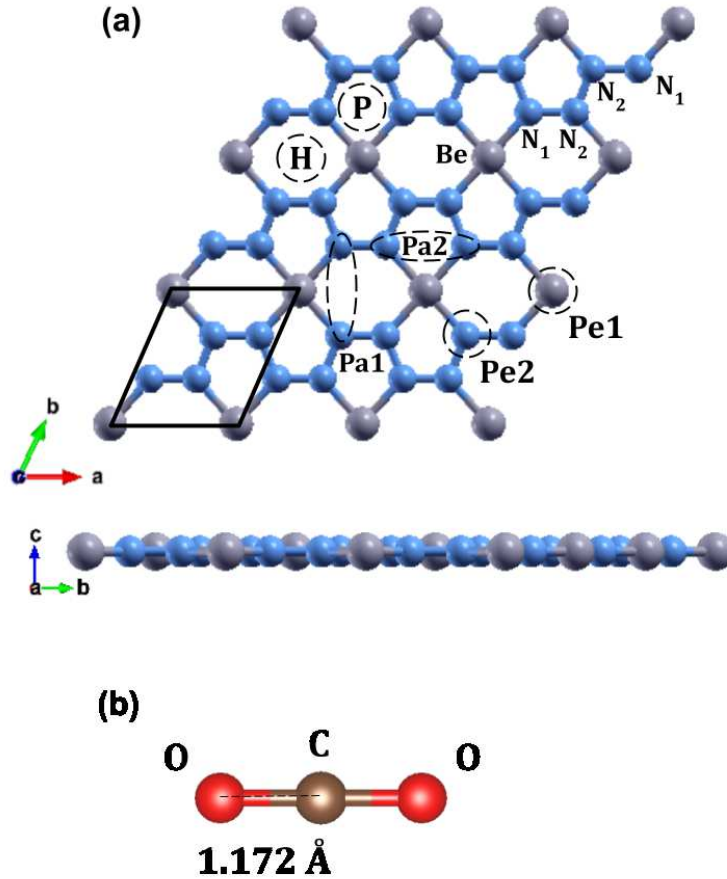


FIG. 2: (a) Atomic structure of a 3×3 supercell of monolayer beryllonitrene (grey atoms are beryllium, and blue atoms are nitrogen). On the beryllonitrene supercell, the CO₂ adsorption sites are labeled Pa1, Pa2, Pe1, and Pe2, and the interstitial doping sites are labeled as H and P. Sites Pa1 and Pa2 are with the CO₂ parallel to the beryllonitrene monolayer, while sites Pe1 and Pe2 are with the CO₂ perpendicular to the beryllonitrene monolayer. Site H is located above the Be₂N₄ hexagon while site P is located above the BeN₄ pentagon. (b) Optimized atomic structure of a single carbon dioxide molecule (red atoms are oxygen, and brown atoms are carbon).

2. Carbon Dioxide Adsorption on Pristine Beryllonitrene

In order to find the most optimal binding site for carbon dioxide, we tested the four beryllonitrene adsorption sites shown in Figure 2(a): Pa1, Pa2, Pe1, and Pe2.

Full relaxation calculations were performed for each configuration of beryllonitrene and carbon dioxide. The relaxed values were used to perform total energy calculations for the relaxed configuration. For the first two configurations, Pa1 and Pa2, we placed the carbon dioxide molecule horizontally above the beryllonitrene such that the oxygen atoms of carbon dioxide were above the nitrogen atoms in beryllonitrene, as shown in Figure 2(a). Position Pa1 for CO₂ is above the BeN₄ pentagon and parallel to the a axis. Position Pa2 for CO₂ is above the Be₂N₄ hexagon and perpendicular to the a axis.

In the next two configurations, Pe1 and Pe2, the carbon dioxide was placed perpendicular to the plane of the two-dimensional beryllonitrene, as shown in Figure 2(a). Position Pe1 for CO₂ is above a beryllium atom, and Position Pe2 for CO₂ is above a nitrogen atom.

TABLE III: Adsorption energy (E_{ads}) for CO₂, distance between CO₂ and beryllonitrene (d), and CO₂ bond angle ($\angle O-C-O$) after adsorption onto pristine beryllonitrene at positions Pa1, Pa2, Pe1, and Pe2 as shown in Figure 3

Position	E_{ads} (Ha)	d (Å)	$\angle O-C-O$ (°)
Pa1	-0.0016	3.91	180
Pa2	-0.0017	3.80	180
Pe1	0.0000	3.29	180
Pe2	0.0000	3.40	180

The relaxed atomic structure for all four configurations is shown in Figure 3. In all 4 configurations, the bond angle of carbon dioxide stayed at around 180°. The most optimal position for carbon dioxide adsorption on beryllonitrene was found to be position Pa2, which was 3.80 Å above the BeN₄ pentagon and perpendicular to the a axis, as shown in Figure 3(b). This configuration has an adsorption energy of -0.0017 Hartree, which is smaller than the chemisorption threshold of -0.011 Ha. For comparison, the adsorption energy for carbon dioxide on pristine boron nitride is -0.0018 Ha¹⁷. This suggests that the carbon dioxide molecule is only physically adsorbed onto the surface of pristine beryllonitrene. Since

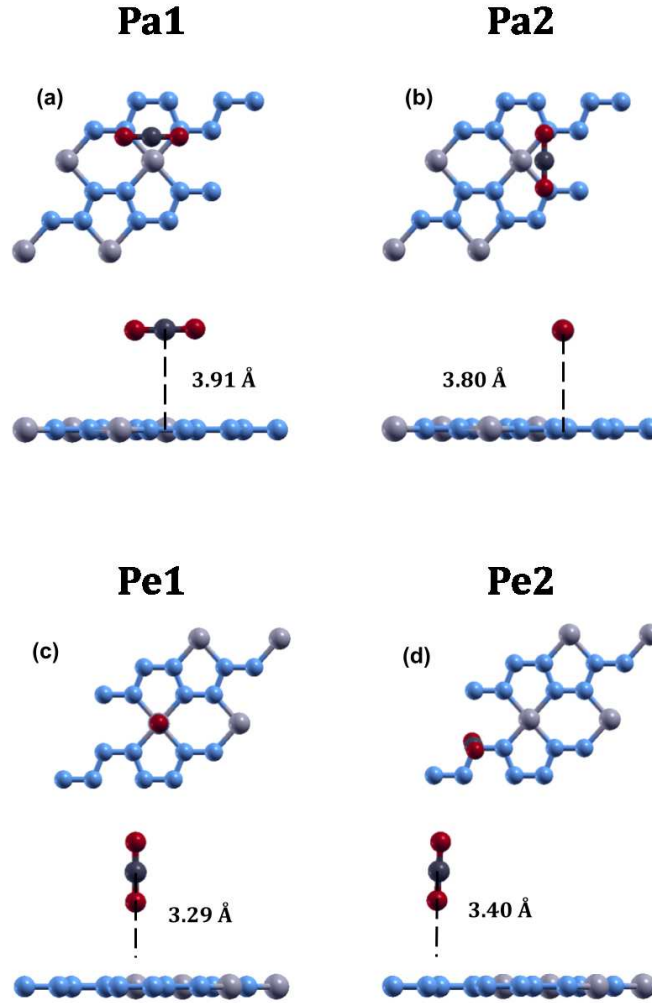


FIG. 3: Optimized atomic configuration for the adsorption of carbon dioxide on pristine beryllonitrene at (a) position Pa1 (Parallel to BeN_4 & above Be_2N_4 hexagon), (b) position Pa2 (Parallel to BeN_4 & above BeN_4 pentagon), (c) position Pe1 (Perpendicular to BeN_4 & above beryllium), and (d) position Pe2 (Perpendicular to BeN_4 & above nitrogen) after relaxation. The blue atoms are nitrogen, the grey atoms are beryllium, the red atoms are oxygen, and the dark grey atoms are carbon.

all of the configurations of carbon dioxide on pristine beryllonitrene had adsorption energies smaller than -0.011 Hartree^{10,23}, this means that carbon dioxide cannot spontaneously chemisorb onto the beryllonitrene, and pristine beryllonitrene is not a viable adsorbent for CO_2 capture.

3. Adsorption of Dopants onto Beryllonitrene Monolayer

We tested the adsorption of Li, Ca, and Al onto beryllonitrene as dopants. In previous experiments, it was found that there are 2 optimal binding sites for ions on beryllonitrene: Site H (above the Be_2N_4 hexagon) and Site P (above the BeN_4 pentagon)⁵⁵ as shown in Figure 2(a). Relaxation calculations were performed for beryllonitrene with the dopants at both H and P.

The relaxed atomic structures for each of the doped beryllonitrene supercells are shown in Figure 4 & 5. When placed at H, all three of the dopants appeared to stay in the same spot. When placed on site P, the dopants tended to move perpendicular to the a axis towards site H. When Al was placed on site P, the Al atom actually moved all the way to site H. The total energy for each of the dopant-beryllonitrene complexes was greater when the dopant was placed at H rather than P. Adsorption of Ca and Al on both sites resulted in positive adsorption energies, which suggests that Ca and Al atoms would prefer to form metallic clusters rather than adsorb to the surface of beryllonitrene⁵⁵ at these two sites. On the other hand, Li has negative adsorption energies at both sites, so it is likely to adsorb to the surface of beryllonitrene. On site H, Li had an adsorption energy of -0.0192 Ha, while Li on site P had an adsorption of energy of -0.0121 Ha. Both of these adsorption energies are greater than -0.011 Hartree, which is considered the chemisorption threshold^{10,23}, so Li is considered to be chemically adsorbed onto beryllonitrene on both of these sites. Since Li had greater adsorption energy on site 1 than on site 2, $\text{Li(H)}\text{-BeN}_4$ is more stable than $\text{Li(P)}\text{-BeN}_4$ (shown in Figure 4).

4. Carbon Dioxide Adsorption on Doped Beryllonitrene

Carbon dioxide adsorption calculations were performed on $\text{Li(H)}\text{-BeN}_4$ as it was found to be the most stable doped form of beryllonitrene that was tested, as shown in Figure 4(a). Three sites on Li-doped beryllonitrene were tested for CO_2 adsorption as shown in Figure 6. Position Pa_C is horizontal with the carbon atom directly above the lithium atom. Position Pa_O is horizontal with an oxygen atom directly above the lithium atom. Position Pe_O is vertical directly above the lithium atom.

Of these three positions, CO_2 molecules only chemisorbed to the Li-doped berylloni-

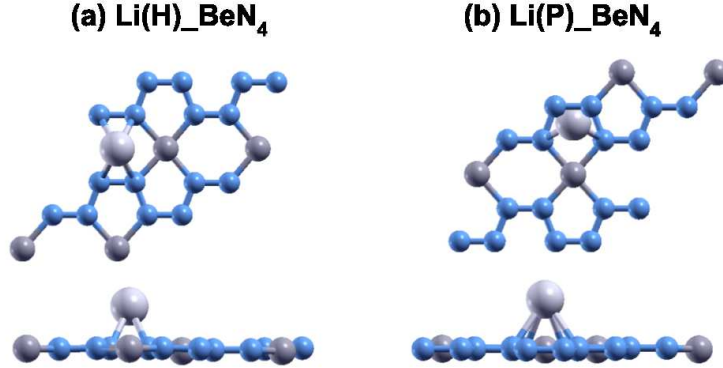


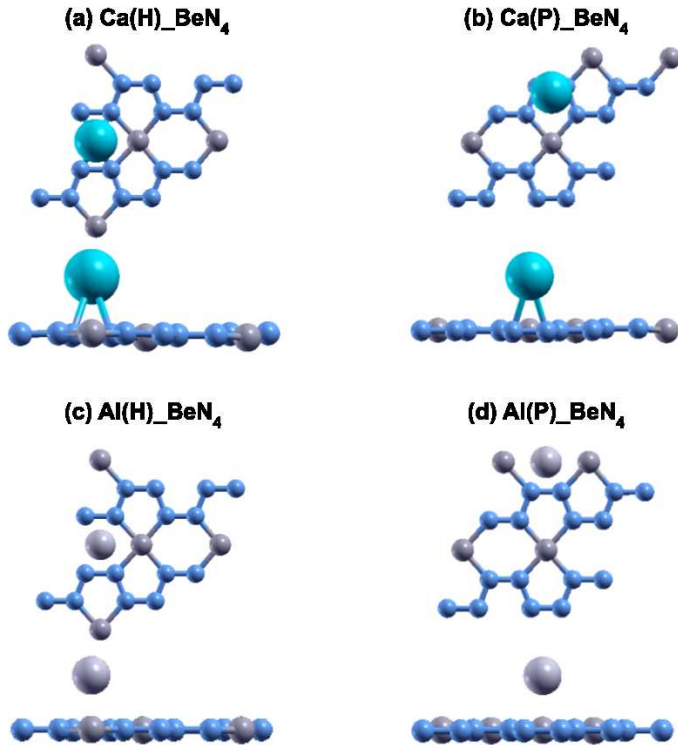
FIG. 4: Optimized atomic structure of beryllonitrene 2×2 supercell doped with Li at (a) H (above the center of the Be_2N_4 hexagon) and at (b) P (above the center of the BeN_4 pentagon) after relaxation. The blue atoms are nitrogen, the dark grey atoms are beryllium, and the light grey atoms are lithium.

TABLE IV: Defect formation energies (E_{def}) and height from beryllonitrene (h) for the following dopants on beryllonitrene: Lithium at site H and site P (Figure 4), as well as Calcium and Aluminum at site H and site P (Figure 5)

Complex	E_{def} (Ha)	h (\AA)
Li_H_BeN ₄	-0.0192	1.49
Li_P_BeN ₄	-0.0121	1.76
Ca_H_BeN ₄	0.0498	2.05
Ca_P_BeN ₄	0.0489	2.26
Al_H_BeN ₄	0.0141	2.00
Al_P_BeN ₄	0.0142	2.01

trene when placed in positions Pa_O and Pe_O. The adsorption energy for CO_2 at position Pa_C is 0.0002 Ha, which is positive, suggesting that this is not a viable position for carbon dioxide to adsorb onto beryllonitrene. In this position, the oxygen atoms were pulled closer to the lithium atom than the carbon atom, resulting in a bond angle of 142.192° . The adsorption energy for CO_2 at position Pa_O is -0.0155 Ha, while the adsorption energy for CO_2 at position Pe_O is -0.0145 Ha. Both of these adsorption energies are greater than the chemisorption threshold of 0.011 Ha, so the CO_2 molecule is chemisorbed to Li-doped

FIG. 5: Optimized atomic structure of beryllonitrene doped with Ca at (a) H and (b) P, as well as beryllonitrene doped with Al at (c) H and (d) P after relaxation. Positions H (above the center of the Be_2N_4 hexagon) and P (above the center of the BeN_4 pentagon) are shown in Figure 2(a). The blue atoms are nitrogen, the dark grey atoms are beryllium, the turquoise atoms are calcium, and the light grey atoms are aluminum.



beryllonitrene at these two positions^{10,23}. This suggests that the oxygen atoms in the CO_2 molecules are attracted to the Li dopant, so CO_2 molecules are more likely to adsorb to Li-doped beryllonitrene with an oxygen atom pointed towards the lithium atom.

Position	E_{ads} (Ha)	d (\AA)	$\angle\text{O-C-O}$ ($^\circ$)
Pa_C	0.0002	2.15	142
Pa_O	-0.0155	1.91	153
Pe_O	-0.0145	1.90	165

TABLE V: Adsorption energies (E_{ads}) for CO_2 , distance between CO_2 and lithium (d), and CO_2 bond angle ($\angle\text{O-C-O}$) on Li-doped beryllonitrene at positions Pa_C, Pa_O, and Pe_O

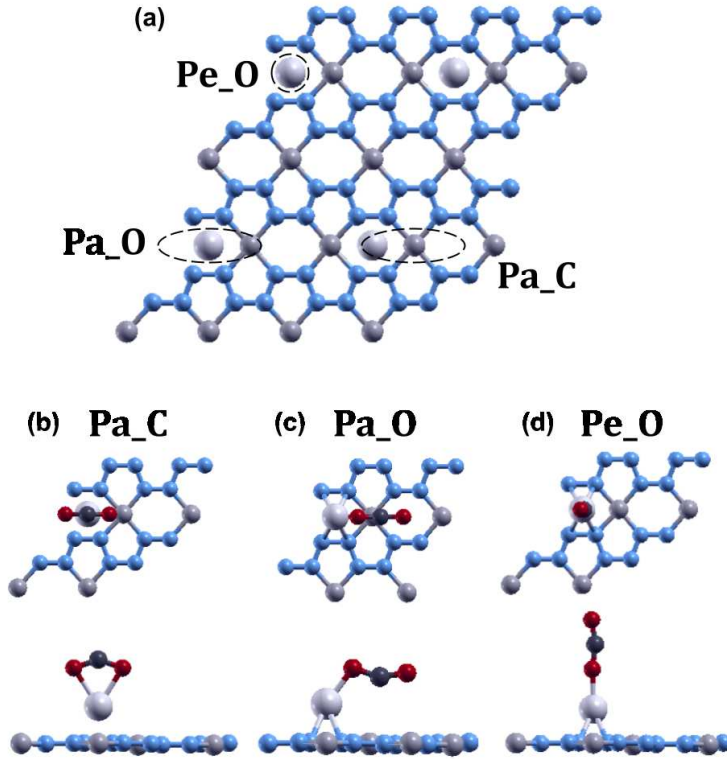


FIG. 6: (a) Three positions for carbon dioxide adsorption on Li-doped beryllonitrene. Optimized structure of carbon dioxide placed onto Li-doped beryllonitrene at positions (b) Pa_C (Parallel to BeN₄ & carbon atom above lithium) (c) Pa_O (Parallel to BeN₄ & oxygen atom above lithium) and (d) Pe_O (Perpendicular to BeN₄ & above lithium). The blue atoms are nitrogen, the medium grey atoms are beryllium, the light grey atoms are lithium, the red atoms are oxygen, and the dark grey atoms are carbon.

Since CO₂ had the greatest adsorption energy when placed in position Pa_O, this configuration appears to be the most stable configuration, so it was used for further calculations.

B. Charge Transfer

The charge transfer diagram was plotted for the adsorption of CO₂ onto Li-doped beryllonitrene at site Pa_O, as shown in Figure 7. There appears to be a transfer of electrons away from the carbon atom and towards the oxygen atoms, particularly the atom facing the

lithium dopant. This makes sense because oxygen is much more electronegative than carbon and lithium, so it has a much stronger attraction towards the electrons. The existence of the charge transfer indicates that a chemical bond was formed between the carbon dioxide molecule and the Li-doped beryllonitrene.

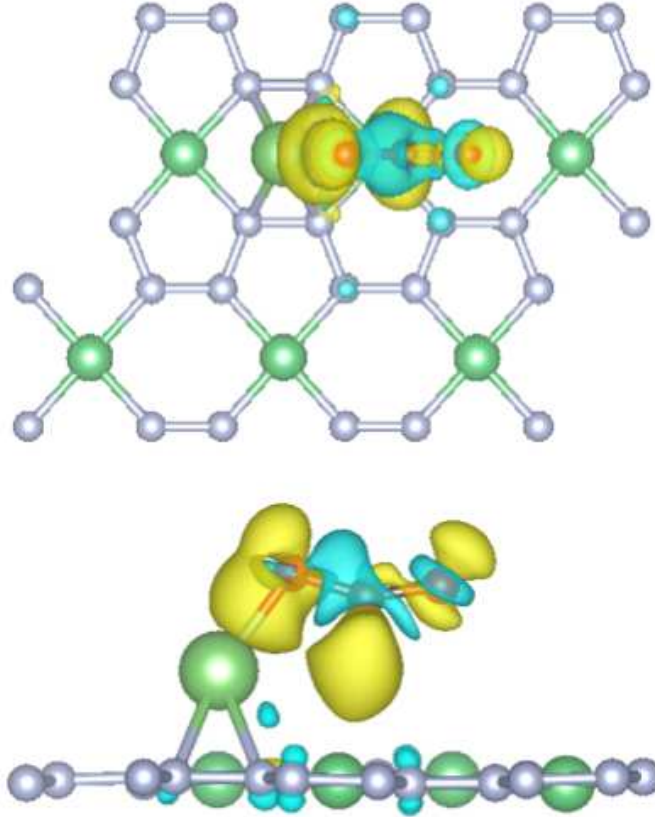


FIG. 7: Top and side view of charge transfer isosurface for adsorption of CO_2 on Li-doped beryllonitrene. Yellow areas are charge gained and blue areas are charge lost.

C. PDOS

To further understand the adsorption of CO_2 onto Li-doped beryllonitrene, the projected density of states (PDOS) was plotted for pristine beryllonitrene, Li-doped beryllonitrene with Li at position H as shown in Figure 2(a), and Li-doped beryllonitrene with carbon dioxide at Pa_O as shown in Figure 6(a).

For pristine beryllonitrene, the 2p orbital of nitrogen (green line) and the 2s orbital for

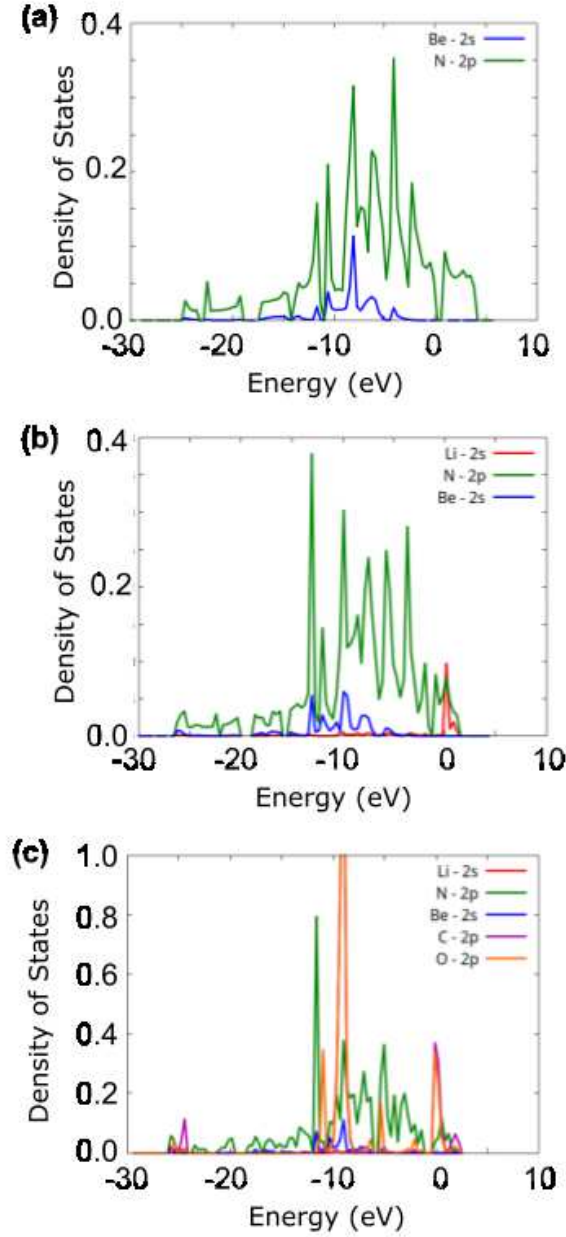


FIG. 8: Projected density of states (PDOS) for (a) pristine beryllonitrene, (b) Li-doped beryllonitrene, and (c) Li-doped beryllonitrene with carbon dioxide adsorbed.

beryllium (blue line) were plotted, as shown in Figure 8(a). There appears to be significant overlap between the 2p orbital of nitrogen and the 2s orbital of beryllium in the range from about -10 to -5 eV. This overlap indicates that the beryllium and nitrogen atoms in the beryllonitrene monolayer are chemically bonded, which means that the beryllonitrene monolayer is a plausible monolayer.

For Li-doped beryllonitrene, the 2s orbital of lithium (red line) was also plotted alongside nitrogen and beryllium, as shown in Figure 8(b). The addition of the lithium dopant causes the PDOS to shift towards the left (towards negative energy). The PDOS for the 2s orbital of lithium (red line) has a major peak at around 0 eV, which overlaps with the PDOS spectra of nitrogen, indicating that a chemical bond has formed between the lithium dopant and the nitrogen in beryllonitrene. Lithium does not demonstrate much overlap with beryllium. This matches with the relaxed atomic structure because it shows that lithium was bonded to beryllonitrene via the four nitrogen atoms in the Be_2N_4 hexagon, as shown in Figure 4(a).

The PDOS spectra was also plotted for the Li-doped beryllonitrene with a carbon dioxide molecule adsorbed at Pa_O, as shown in Figure 8(c). In addition to the spectra for lithium, nitrogen, and beryllium, the 2p orbitals of oxygen (orange line) and carbon (purple line) were also plotted. Lithium's largest peaks were located at around 2 and -10 eV, and had significant overlap with the carbon and oxygen molecules at these peaks. This suggests that the carbon dioxide molecule was chemically bonded to the lithium atom. The PDOS spectra of nitrogen also overlapped with lithium at these peaks, indicating that the lithium dopant was still bound to the beryllonitrene. These results show that carbon dioxide was able to successfully chemically bond to Li-doped beryllonitrene.

D. Band Structure

In order to better understand the electronic properties of the materials, the band structure was plotted for pristine beryllonitrene, Li-doped beryllonitrene, and Li-doped beryllonitrene with CO_2 adsorbed at Pa_O. Figure 9 shows the calculated band structures for these materials.

The calculated band structure for a 2x2 supercell of pristine beryllonitrene is in Figure 9(a), and it shows that beryllonitrene is a zero-gap semimetal with a Dirac-point between the A and Y k-points, which is consistent with previous results⁴¹. The band structure for Li-doped beryllonitrene shown in Figure 9(b) shows that after the lithium dopant is added to the beryllonitrene, the half-filled band from lithium lies entirely above the Fermi level. This means that lithium doping changes beryllonitrene from a semimetal to a metal.

Figure 9(c) shows the band structure of Li-doped beryllonitrene after carbon dioxide is adsorbed at site Pa₁O. The two bands above the Fermi level appear to have been changed significantly, indicating that the adsorption of CO₂ changes the electronic structure of Li-doped beryllonitrene.

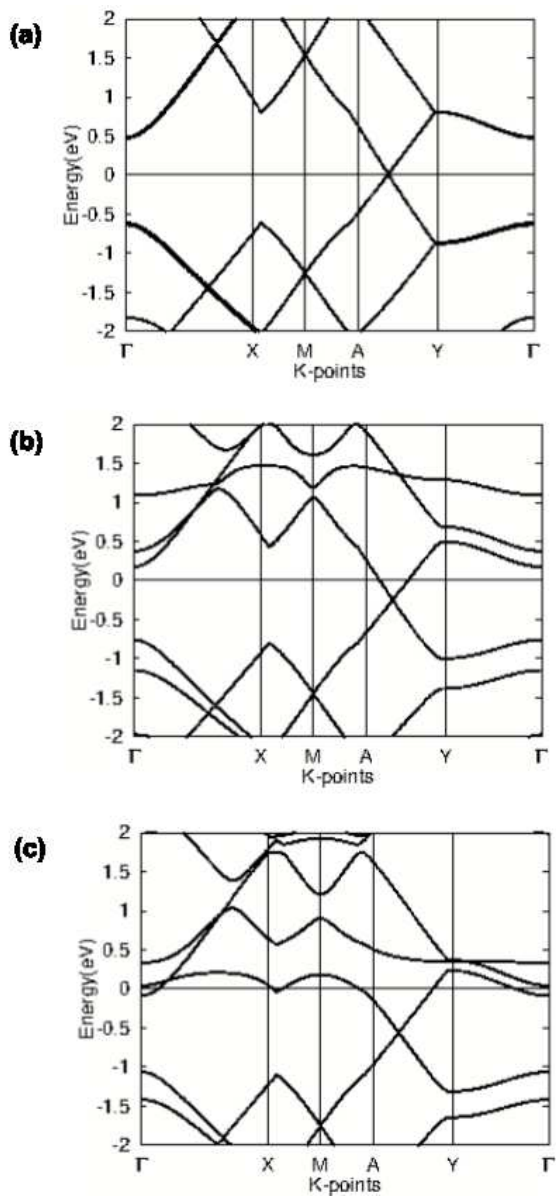


FIG. 9: Band structure for (a) pristine beryllonitrene, (b) Li-doped beryllonitrene, and (c) Li-doped beryllonitrene with carbon dioxide adsorbed.

Since Li-doped beryllonitrene exhibits metallic behavior, it could potentially be used as a charge-modulated CO₂ capture material. Several other metallic materials have already

been theoretically tested for charge-modulated CO₂ capture^{27,57}.

IV. CONCLUSION

In summary, we used first principle calculations to determine the carbon dioxide capture ability of pristine beryllonitrene and Li-doped beryllonitrene. The atomic structure, adsorption energy, charge transfer, projected density of states, and band structure were analyzed to determine the viability of carbon dioxide adsorption. We found that pristine beryllonitrene demonstrated very weak attraction towards carbon dioxide. In order to enhance the carbon dioxide adsorption ability, we doped beryllonitrene with three different dopants: lithium, calcium, and aluminum. Calcium and aluminum were unable to spontaneously adsorb, but lithium was able to strongly chemisorb onto pristine beryllonitrene, producing Li-doped beryllonitrene. Lithium doping appeared to greatly enhanced the carbon dioxide capture ability of beryllonitrene since carbon dioxide had an adsorption energy of -0.0155 Ha on Li-doped beryllonitrene, meaning that the CO₂ molecule was chemisorbed. The charge transfer, projected density of states, and band structure diagrams show that the adsorption of carbon dioxide greatly change the electronic structure of the Li-doped beryllonitrene, suggesting that carbon dioxide is strongly chemisorbed onto the surface. These results demonstrate that Li-doped beryllonitrene is a possible candidate for application in CO₂ capture.

In our study, we did not consider whether or not the adsorption of carbon dioxide on these beryllonitrene monolayers was reversible. Typically, a certain amount of energy is required in order for the carbon dioxide to be removed. Future studies could explore the possibility of charge-controlled or strain-controlled CO₂ capture using beryllonitrene for easier regeneration. Additionally, the calculations performed in this study were only theoretical. In the future, these results can be applied to experimental carbon dioxide adsorbents. In order to maximize the abilities of beryllonitrene, future research could also be done to investigate the effects of vacancies and other dopants on the CO₂ capture ability of beryllonitrene.

-
- ¹ T. J. Crowley, *Science* **289**, 270 (2000).
- ² E. G. G. Emissions and C. Change, Available at:[Google Scholar] (2017).
- ³ E. Bekkers, J. F. Francois, and H. Rojas-Romagosa, *The Economic Journal* **128**, 1095 (2018).
- ⁴ M. Benzie, A. Harvey, K. Burningham, N. Hodgson, and A. Siddiqi, York, UK: The Joseph Rowntree Foundation (2011).
- ⁵ Q. Zhou, J. Koiwanit, L. Piewkhaow, A. Manuilova, C. Chan, M. Wilson, and P. Tontiwachwuthikul, *Energy Procedia* **63**, 7452 (2014).
- ⁶ M. Kanniche, R. Gros-Bonnivard, P. Jaud, J. Valle-Marcos, J.-M. Amann, and C. Bouallou, *Applied Thermal Engineering* **30**, 53 (2010).
- ⁷ C.-H. Yu, C.-H. Huang, C.-S. Tan, et al., *Aerosol and Air Quality Research* **12**, 745 (2012).
- ⁸ G. T. Rochelle, *Science* **325**, 1652 (2009).
- ⁹ R. S. Haszeldine, *Science* **325**, 1647 (2009).
- ¹⁰ S. A. Tawfik, X. Cui, S. Ringer, and C. Stampfl, *RSC Advances* **5**, 50975 (2015).
- ¹¹ M. Ishibashi, H. Ota, N. Akutsu, S. Umeda, M. Tajika, J. Izumi, A. Yasutake, T. Kabata, and Y. Kageyama, *Energy conversion and management* **37**, 929 (1996).
- ¹² Y. Takamura, J. Aoki, S. Uchida, and S. Narita, *The Canadian Journal of Chemical Engineering* **79**, 812 (2001).
- ¹³ B. Metz, O. Davidson, H. De Coninck, M. Loos, and L. Meyer, *IPCC special report on carbon dioxide capture and storage* (Cambridge: Cambridge University Press, 2005).
- ¹⁴ K. S. Novoselov, A. K. Geim, S. V. Morozov, D.-e. Jiang, Y. Zhang, S. V. Dubonos, I. V. Grigorieva, and A. A. Firsov, *science* **306**, 666 (2004).
- ¹⁵ B. Shivananju, H. Y. Hoh, W. Yu, and Q. Bao, in *Fundamentals and Sensing Applications of 2D Materials* (Elsevier, 2019), pp. 379–406.
- ¹⁶ T. Wehling, K. Novoselov, S. Morozov, E. Vdovin, M. Katsnelson, A. Geim, and A. Lichtenstein, *Nano letters* **8**, 173 (2008).
- ¹⁷ Y. Jiao, A. Du, Z. Zhu, V. Rudolph, G. Q. M. Lu, and S. C. Smith, *Catalysis today* **175**, 271 (2011).
- ¹⁸ S. M. Aghaei, M. Monshi, I. Torres, M. Banakermani, and I. Calizo, *Physics Letters A* **382**,

- 334 (2018).
- ¹⁹ T. Hussain, T. Kaewmaraya, S. Chakraborty, and R. Ahuja, *The Journal of Physical Chemistry C* **120**, 25256 (2016).
- ²⁰ W. Xia, W. Hu, Z. Li, and J. Yang, *Physical Chemistry Chemical Physics* **16**, 22495 (2014).
- ²¹ N. Yu, L. Wang, M. Li, X. Sun, T. Hou, and Y. Li, *Physical Chemistry Chemical Physics* **17**, 11700 (2015).
- ²² Q. Sun, G. Qin, Y. Ma, W. Wang, P. Li, A. Du, and Z. Li, *Nanoscale* **9**, 19 (2017).
- ²³ K. Jia and X. Luo, *PeerJ Materials Science* **2**, e3 (2020).
- ²⁴ G. Rao, T. Hussain, M. S. Islam, M. Sagynbaeva, D. Gupta, P. Panigrahi, and R. Ahuja, *Nanotechnology* **27**, 015502 (2015).
- ²⁵ Y. Yong, X. Su, H. Cui, Q. Zhou, Y. Kuang, and X. Li, *ACS omega* **2**, 8888 (2017).
- ²⁶ X. Fu, H. Yang, L. Fu, C. He, J. Huo, J. Guo, and L. Li, *Chinese Chemical Letters* **32**, 1089 (2021).
- ²⁷ H. Zhang, H. Xiong, and W. Liu, *Crystals* **11**, 543 (2021).
- ²⁸ M. H. Darvishnejad and A. Reisi-Vanani, *Computational Materials Science* **176**, 109539 (2020).
- ²⁹ M. H. Darvishnejad and A. Reisi-Vanani, *Journal of CO2 Utilization* **46**, 101469 (2021).
- ³⁰ S. Zhou, M. Wang, S. Wei, S. Cao, Z. Wang, S. Liu, D. Sun, and X. Lu, *Materials Today Physics* **16**, 100301 (2021).
- ³¹ W. Luo, H. Wang, Z. Wang, G. Liu, S. Liu, and C. Ouyang, *Physical Chemistry Chemical Physics* **22**, 8864 (2020).
- ³² X. Tan, L. Kou, H. A. Tahini, and S. C. Smith, *Scientific reports* **5**, 1 (2015).
- ³³ G. Qin, Q. Cui, W. Wang, P. Li, A. Du, and Q. Sun, *ChemPhysChem* **19**, 2788 (2018).
- ³⁴ C. He, M. Zhang, T. Li, and W. Zhang, *Applied Surface Science* **505**, 144619 (2020).
- ³⁵ C. He, M. Zhang, T. Li, and W. Zhang, *Journal of Materials Chemistry C* **8**, 6542 (2020).
- ³⁶ J. Li, M. Hou, Y. Chen, W. Cen, Y. Chu, and S. Yin, *Applied Surface Science* **399**, 420 (2017).
- ³⁷ V. Chandra, S. U. Yu, S. H. Kim, Y. S. Yoon, D. Y. Kim, A. H. Kwon, M. Meyyappan, and K. S. Kim, *Chemical communications* **48**, 735 (2012).
- ³⁸ Y. Liu, L. Li, Q. Li, J. Lin, Z. Guo, X. Zhang, Z. Lu, Y. Ma, Y. Huang, and C. Tang, *Applied Surface Science* **556**, 149775 (2021).
- ³⁹ J. Zhu, A. Chronos, and U. Schwingenschlögl, *physica status solidi (RRL)–Rapid Research*

- Letters **10**, 458 (2016).
- ⁴⁰ M. Bykov, T. Fedotenko, S. Chariton, D. Laniel, K. Glazyrin, M. Hanfland, J. S. Smith, V. B. Prakapenka, M. F. Mahmood, A. F. Goncharov, et al., Physical Review Letters **126**, 175501 (2021).
- ⁴¹ A. Bafekry, C. Stampfl, M. Faraji, M. Yagmurcukardes, M. Fadlallah, H. Jappor, M. Ghergherehchi, and S. Fegghi, Applied Physics Letters **118**, 203103 (2021).
- ⁴² W. Kohn and L. J. Sham, Physical review **140**, A1133 (1965).
- ⁴³ P. Hohenberg and W. Kohn, Physical review **136**, B864 (1964).
- ⁴⁴ X. Gonze, B. Amadon, G. Antonius, F. Arnardi, L. Baguet, J.-M. Beuken, J. Bieder, F. Bottin, J. Bouchet, E. Bousquet, et al., Computer Physics Communications **248**, 107042 (2020).
- ⁴⁵ A. H. Romero, D. C. Allan, B. Amadon, G. Antonius, T. Applencourt, L. Baguet, J. Bieder, F. Bottin, J. Bouchet, E. Bousquet, et al., The Journal of chemical physics **152**, 124102 (2020).
- ⁴⁶ X. Gonze, F. Jollet, F. A. Araujo, D. Adams, B. Amadon, T. Applencourt, C. Audouze, J.-M. Beuken, J. Bieder, A. Bokhanchuk, et al., Computer Physics Communications **205**, 106 (2016).
- ⁴⁷ X. Gonze, B. Amadon, P.-M. Anglade, J.-M. Beuken, F. Bottin, P. Boulanger, F. Bruneval, D. Caliste, R. Caracas, M. Côté, et al., Computer Physics Communications **180**, 2582 (2009).
- ⁴⁸ X. Gonze, Zeitschrift für Kristallographie-Crystalline Materials **220**, 558 (2005).
- ⁴⁹ X. Gonze, J.-M. Beuken, R. Caracas, F. Detraux, M. Fuchs, G.-M. Rignanese, L. Sindic, M. Verstraete, G. Zerah, F. Jollet, et al., Computational Materials Science **25**, 478 (2002).
- ⁵⁰ J. P. Perdew, K. Burke, and M. Ernzerhof, Physical review letters **77**, 3865 (1996).
- ⁵¹ P. E. Blöchl, Physical review B **50**, 17953 (1994).
- ⁵² M. Torrent, F. Jollet, F. Bottin, G. Zérah, and X. Gonze, Computational Materials Science **42**, 337 (2008).
- ⁵³ N. Holzwarth, A. Tackett, and G. Matthews, Computer Physics Communications **135**, 329 (2001).
- ⁵⁴ J. D. Head and M. C. Zerner, Chemical physics letters **122**, 264 (1985).
- ⁵⁵ B. Mortazavi, F. Shojaei, and X. Zhuang, Materials Today Nano p. 100125 (2021).
- ⁵⁶ A. Klotz, T. Ward, and E. Dartois, Astronomy & Astrophysics **416**, 801 (2004).
- ⁵⁷ X. Tan, H. A. Tahini, and S. C. Smith, ACS applied materials & interfaces **9**, 19825 (2017).